ELSEVIER

Journal of Chromatography A, 802 (1998) 49–57

JOURNAL OF CHROMATOGRAPHY A

Numerical simulation for capillary electrophoresis I. Development of a simulation program with high numerical stability

Natsuki Ikuta*, Takeshi Hirokawa

Applied Physics and Chemistry, Faculty of Engineering, Hiroshima University, Kagamiyama 1, Higashi-Hiroshima 739, Japan

Abstract

A computer program was developed for the simulations of capillary electrophoresis on the basis of unsteady partial differential equations. Since a new algorithm (shifted upwinding approximation) was used to suppress numerical divergence and oscillation, the program succeeded in generating only physically meaningful peaks at the cost of slight overestimation of ionic diffusion. The mathematical model and equations used in the program were described in detail, and simulation performance was compared among the previously reported programs, confirming the numerical stability of our program. As an application example, a system peak in indirect UV detection was simulated. © 1998 Published by Elsevier Science B.V.

Keywords: Computer simulation; Mathematical modelling

1. Introduction

Capillary zone electrophoresis (CZE) is a useful analytical method for ionic substances with high sensitivity and high separability. Although absolute sensitivity of CZE is very high, its analytical reproducibility depends on the sample due to the lack of concentration regulation. That is, the migration time of a sample component may change more or less depending on its concentration, ionic strength of the sample solution and even coexisting counter ions. Since migration time is usually used as a qualitative index and good reproducibility of the index is one of the essential factors of a useful analytical method, it is important to clarify how the nature of the sample solution affects the migration time.

Although the initial stage of migration process of CZE is important to clarify the above, direct observation of the migration process is difficult due to physical restriction. In such case accurate computer simulation may be helpful to estimate what will happen in the sample plug and adjacent background electrolyte (BGE). For the above purpose, we have developed a computer program for the simulation of CE process.

Several computer programs have already been developed for CE simulation [1–7], in which nonlinear partial differential equations are numerically solved for the unsteady state. However, the simulations have some difficulties such as numerical divergence and oscillation causing termination of calculation and/or false (non-physical) peaks. Although 'upwinding' approximation is a useful algorithm to avoid these difficulties, the divergence and/or oscillation would appear [7] depending on the condition of calculation. The non-physical peaks are proble-

*Corresponding author

0021-9673/98/$19.00
PII S0021-9673(97)01284-3

matical especially when they appear at an initial stage of calculation, because they spoil not only accurate simulation of the initial migration process such as sample stacking but also all of the subsequent calculations.

Ermakov et al. has succeeded in rapid simulation of peak profiles in consideration of a term eliminating numerical dispersion with less numerical divergence and oscillation using an 'upwinding' algorithm [6]. However, some problems remain: that negative concentration zones were generated before and behind the sample peaks and the peak profiles were distorted by non-physical peaks [6,7]. Although these non-physical zones can be suppressed by using low potential gradient, small space step and time step in the calculation of finite difference, obviously such a simulation calculation will be time-consuming and not useful.

Taking into account the above problems in CE simulation, in this paper we propose a 'shifted upwinding' method to suppress non-physical peaks caused by oscillations. In this method, variables which have not been upwinded in the former methods were shifted in consideration of physical phenomena. Consequently, divergence and oscillation have hardly been raised at the cost of slight overestimation of ionic diffusion. After describing the details of the mathematical model, the performance of the developed program is discussed in comparison with previous one [??]. Finally a system peak in CZE is simulated and visualized as an application example.

2. Theoretical

2.1. Equation of continuity

The continuity equation for ith ionic species with absolute mobility m_i can be written as follows:

$$\frac{\partial C_i(x,t)}{\partial t} = D_i \frac{\partial^2 C_i(x,t)}{\partial x^2} - \frac{\partial}{\partial x}\{v_i(x,t)C_i(x,t)\} \qquad (1)$$

where $C_i(x,t)$, D_i and $v_i(x,t)$ are the concentration, the diffusion constant and the migration velocity, x the axis coordinate along the capillary and t the time coordinate. The migration velocity of ith ionic species is written as:

$$v_i(x,t) = (\overline{m_i(x,t)} + m_{\mathrm{eof}})E(x,t)$$

where $\overline{m_i(x,t)}$ and m_{eof} are the effective mobility of ith ionic species and mobility of electroosmotic flow (EOF), and $E(x,t)$ is the potential gradient at the position x and time t. This equation of continuity is valid not only for the sample ions but also for background ions. That is, if an integral of Eq. (1) is obtained, behaviors of the supporting electrolyte as well as the samples are comprehended.

Neglecting the quadratic term in Eq. (1) and using Kohlrausch's regulating functions [8], Mikkers et al. obtained analytical solutions of Eq. (1) and showed that electrophoretic dispersions arose from changes in potential gradient at a sample zone [9]. This conclusion is of course valid, however it should be noted that the regulating function was obtained by neglecting the diffusional dispersion and by using the assumption that the effective mobility of a sample was constant in its zone during migration process. However, in the practical zone, conductivity and potential gradient are not constant. That is, these may change according to the concentration distribution of the constituents in the zone. Moreover, effective mobility of the constituents can change, because the pH may not be constant in the zone according to the concentration distribution of the constituents. Taking into account these facts, we did not use Kolrausch's regulating function in our simulation calculation. Taking into account the above variation of the effective mobility, potential gradient and concentration for accurate simulation, Eq. (1) can be rewritten as follows:

$$\frac{\partial C_i}{\partial t} = D_i \frac{\partial^2 C_i}{\partial x^2} - \left\{ EC_i \frac{\partial \overline{m_i}}{\partial x} + (\overline{m_i} + m_{\mathrm{eof}})C_i \frac{\partial E}{\partial x} + (\overline{m_i} + m_{\mathrm{eof}})E \frac{\partial C_i}{\partial x} \right\} \qquad (2)$$

Since it is difficult to solve analytically such a nonlinear partial differential equation for unsteady state, as in Eq. (2), we have to solve it numerically using a computer.

2.2. Effective mobility

For convenience, the constituent ions are limited

as univalent ones. The effective mobility of ith ionic species (m_i) is expressed as:

$$\overline{m_i}(x,t) = \alpha_i(x,t)m_i \tag{3}$$

where $\alpha_i(x,t)$ is the degree of dissociation. According to law of conservation of mass and electroneutrality, the following equation of $C_i(x,t)$ and proton concentration ($[H^+]$) is obtained:

$$\sum_{\text{cation}} \frac{[H^+](x,t)C_i(x,t)}{[H^+](x,t)+K_{ai}} - \sum_{\text{anion}} \frac{K_{ai}C_i(x,t)}{[H^+](x,t)+K_{ai}} + [H^+](x,t) - \frac{K_w}{[H^+](x,t)} = 0 \tag{4}$$

where K_{ai} is the acid dissociation constant of ith ionic species and K_w is ion product of water. The proton concentration is obtained by solving Eq. (4) to estimate α_i according to the following equation:

$$\alpha_i(x,t) = \begin{cases} \dfrac{[H^+](x,t)}{[H^+](x,t)+K_i} & \text{(cation)} \\ \dfrac{K_i}{[H^+](x,t)+K_i} & \text{(anion)} \end{cases} \tag{5}$$

2.3. Potential gradient

On the assumption that diffusion current is small enough to neglect, conductivity at a given place x, $\Lambda(x)$, is expressed as:

$$\Lambda(x) = F\sum_f |\overline{m_i(x)}|C_i(x) + |m_{H^+}|[H^+](x) + |m_{OH^-}|[OH^-](x) \tag{6}$$

where F is Faraday constant, m_H and m_{OH} are the mobilities of H^+ and OH^-. Accordingly, specific resistance at this place ($\rho(x)$) is obtained in the following form:

$$\rho(x) = 1/\Lambda(x) = \frac{1}{F\left(\sum_i |\overline{m_i(x)}|C_i(x) + |m_{H^+}|[H^+](x) + |m_{OH^-}|[OH^-](x)\right)} \tag{7}$$

The resistance of whole capillary system R is then expressed as

$$R = \int_L \frac{\rho(x)}{\pi r^2}\,dx = \int_L \frac{dx}{\pi r^2 F\left(\sum_i |\overline{m_i(x)}|C_i(x) + |m_{H^+}|[H^+](x) + |m_{OH^-}|[OH^-](x)\right)} \tag{8}$$

where r is a radius of a separation capillary. Supposing migration voltage (V) is applied by using a constant voltage power supply, electric current I through the system is expressed as follows:

$$I = \frac{V}{R} = \frac{V}{\displaystyle\int_L \frac{dx}{\pi r^2 F\left(\sum_i |\overline{m_i(x)}|C_i(x) + |m_{H^+}|[H^+](x) + |m_{OH^-}|[OH^-](x)\right)}} \tag{9}$$

At a given place x, potential gradient $E(x)$ is obtained as follows:

$$E(x,t) = I\rho(x,t)/\pi r^2 = \frac{V}{\displaystyle\int_L \frac{dx}{\left(\sum_i |\overline{m_i}|C_i + |m_{H^+}|[H^+] + |m_{OH^-}|[OH^-]\right)}} \times \frac{1}{\left(\sum_i |\overline{m_i}|C_i + |m_{H^+}|[H^+] + |m_{OH^-}|[OH^-]\right)} \tag{10}$$

When a constant current power supply is used, $E(x)$ is obtained as follows:

$$E(x) = \frac{I}{\pi r^2 F\left(\sum_i |\overline{m_i(x)}|C_i(x) + |m_{H^+}|[H^+](x) + |m_{OH^-}|[OH^-](x)\right)} = \frac{j}{F\left(\sum_i |\overline{m_i(x)}|C_i(x) + |m_{H^+}|[H^+](x) + |m_{OH^-}|[OH^-](x)\right)} \tag{11}$$

where j is current density.

3. Numerical simulation program

3.1. Model of electrophoretic system

Fig. 1 shows the model of the electrophoretic

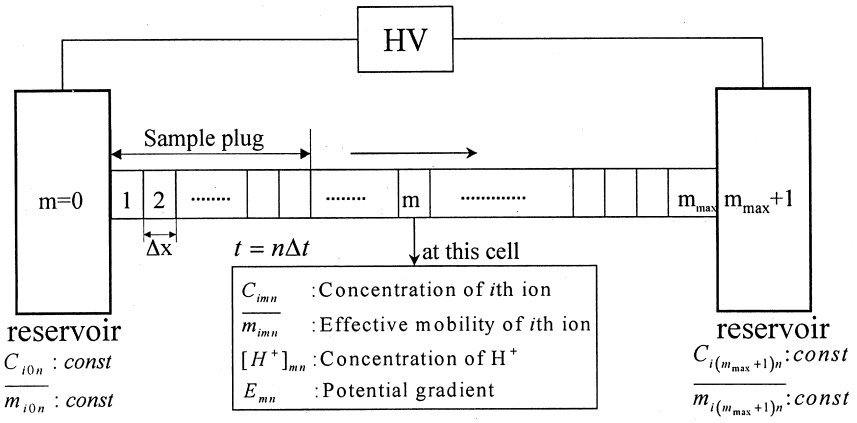

Fig. 1. Model of the electrophoretic system used for simulation. Two reservoirs are connected by a capillary, which is segmented to grids with a space step of Δx. Δt is a space step. HV is a high voltage power supply.

system used for our numerical simulation. Each electrolyte reservoir can hold the same BGE for CZE or different operational electrolyte for the other migration mode such as ITP. During the migration process, the constituents of BGE in the reservoirs cannot change but potential gradient can. For example, when a sample with extremely low conductivity is introduced, the potential gradient becomes high in the sample and that of the rest, including the reservoirs, becomes low.

3.2. Finite-difference equations

For numerical calculation, Eq. (2) must be transformed to finite-difference equations. However, as described in the earlier section, simple transformation results in divergence and/or oscillation for a nonlinear unsteady partial differential equation. In order to obtain numerical stability in such a calculation, as already mentioned, 'upwind' difference approximation with artificial dispersion has been introduced to obtain finite-difference equations by Ermakov et al. [6,7]. Our strategy to avoid divergence and oscillation is enhancing the numerical stability of their 'upwinding' method by using more upstream data than the data used in the previous method. Finite-difference equations used in our calculation were obtained for cationic analysis ($E>0$, $C>0$) as follows:for $\overline{m_{imn}} + m_{\mathrm{eof}} \geq 0$

$$C_{imn+1} = C_{imn} + \frac{D_i \Delta t}{\Delta x^2}(C_{i(m-1)n} - 2C_{imn} + C_{i(m+1)n}) - \frac{\Delta t}{\Delta x}\{(\overline{m_{imn}} - \overline{m_{i(m-1)n}})E_{mn}\underline{C_{i(m-1)n}} + (\overline{m_{imn}} + m_{\mathrm{eof}})(E_{mn} - E_{(m-1)n})\underline{C_{i(m-1)n}} + (\overline{m_{imn}} + m_{\mathrm{eof}})E_{mn}(C_{imn} - C_{i(m-1)n})\} \quad (12a)$$

for $\overline{m_{imn}} + m_{\mathrm{eof}} < 0$

$$C_{imn+1} = C_{imn} + \frac{D_i \Delta t}{\Delta x^2}(C_{i(m-1)n} - 2C_{imn} + C_{i(m+1)n}) = -\frac{\Delta t}{\Delta x}\{(\overline{m_{i(m+1)n}} - \overline{m_{imn}})E_{mn}C_{imn} + (\overline{m_{imn}} + m_{\mathrm{eof}})(E_{(m+1)n} - E_{mn})\underline{C_{i(m+1)n}} + (\overline{m_{imn}} + m_{\mathrm{eof}})\underline{E_{(m+1)n}}(C_{i(m+1)n} - C_{imn})\} \quad (12b)$$

where subscripts i, m, and n show ith ionic species at time $n\Delta t$ and the position $m\Delta x$. Thus, the concentration of the ith ionic species at $t=(n+1)\Delta t$ can be derived from that at $t=n\Delta t$.

In the typical upwinding approximation [2–6], the underlined terms in Eqs. (12a) and (12b) for concentration should be C_{imn}, and those for potential

gradient should be E_{imn}. In the present approximation, their upstream data, i.e. concentration and potential gradient of the adjacent grid ($C_{I(m-1)n}$ and $E_{I(m-1)n}$), were used instead. As shown in a later section, much better numerical stability in simulation calculation was obtained by the use of the present approximation without any further artificial dispersion. Although it was estimated that numerical dispersion inherent in 'upwinding' approximation might increase, the increase was slight. Hereafterm, we call our approximation a 'shifted upwinding' approximation.

3.3. Effective mobility and potential gradient

Effective mobility and potential gradient for Eqs. (12a) and (12b) were derived as follows: at $x=mh$, $t=n\Delta t$, $[H^+]$ is calculated from Eq. (4) by the Newton–Raphson method to estimate α_{imn} from Eq. (5). An effective mobility of ith ion species (m_{imn}) is then derived from Eq. (5). Since this process is time-consuming due to iterative calculation, the simulation speed is determined by this process.

3.4. Potential gradient

Integral of Eq. (8) is transformed to summation as follows:

$$E_{mn} = \frac{V}{h}\cdot\frac{1}{\sum_m \frac{\mathrm{d}x}{\sum_i\left(|\overline{m_{imn}}|C_{imn}+|m_{H^+}|[H^+]_{mn}+|m_{OH^-}|[OH^-]_{mn}\right)}} \times\frac{1}{\sum_i\left(|\overline{m_{imn}}|C_{imn}+|m_{H^+}|[H^+]_{mn}+|m_{OH^-}|[OH^-]_{mn}\right)} \quad (13)$$

4. Experimental

In order to compare the simulation performance of the present program with that previously reported [7], simulation was carried using the migration condition as in Ref. [7]. The supporting electrolyte was 12 m*M* Tris–20 m*M* acetic acid, and the test mixture contained 1 m*M* pyridine and 1 m*M* aniline. It was assumed that the sample plug length was 0.5 cm, the inner diameter of a capillary was 50 μm, the effective length was 9.5 cm and the driving current was 5 μA. Electroosmotic mobility was assumed to be zero. The physicochemical constants of the sample components and BGE constituents are listed in Table 1. The unit cell length (space step) and the time step in the calculation were 0.002 cm and 0.002 s, respectively.

Table 1
Physicochemical constants used in simulations at 25°C

Species	Mobility[a]	pK_a
Aniline	32.5	4.8
Pyridine	30.0	5.18
Tris	24.1	8.3
K	76.2	13.0
Li	40.1	13.8
ϵ-Aminocaproic acid	28.8	4.4
Creatinine	31.0	4.8
Acetic acid	−42.4	4.756
Cl	−79.1	−2

[a]Absolute mobility (10^{-5} cm^2 V^{-1} s^{-1}).

For a demonstration, a system peak in indirect UV detection was simulated. The supporting electrolyte used was 30 m*M* creatinine–30 m*M* acetic acid. The sample solution contained 3 m*M* KCl, 3 m*M* LiCl and 3 m*M* ϵ-aminocaproic acid and the length of injected sample plug was 0.2 cm. The simulation assumed $L=40$ cm, $V=30$ kV, $\Delta x=0.05$ cm, $\Delta x=0.001$ s and $m_{eof}=30.0\times10^{-5}$ cm^2 V^{-1} s^{-1}. Mobility and pK_a of ionic species in the samples and the electrolytes are shown also in Table 1.

All calculations were performed on an IBM compatible with a Pentium 90 MHz and Windows 95. The calculation part of our program was written in ANSI C and the user interface was written in Visual Basic (Microsoft, USA). The output data included concentration of the constituents, pH and potential gradient, etc.

5. Result and discussion

5.1. Comparison with previous programs

The solid line in Fig. 2 shows the electropherogram of pyridine and aniline, which was simulated under the same conditions as Ermakov et al. reported [7] (migration current = 5 μA, potential gradient = 329 V cm^{-1}). In their simulation, small negative

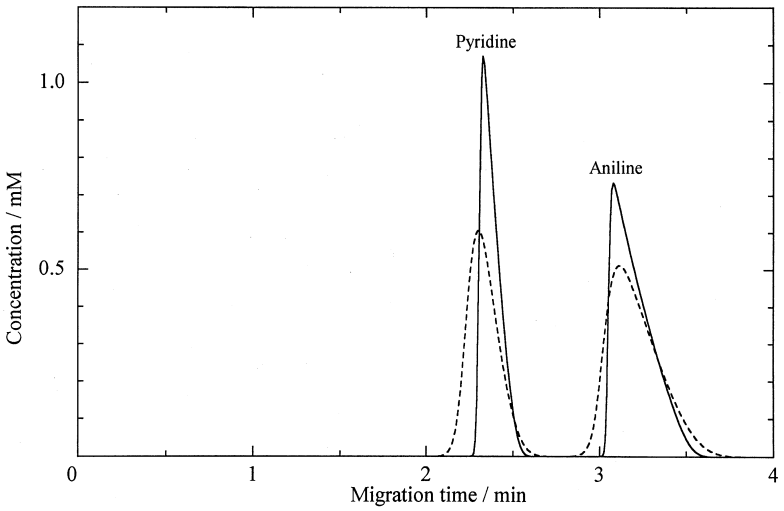

Fig. 2. Concentration profiles of aniline and pyridine in the CZE process simulated by using shifted upwinding approximation. The migration current was 5 μA and potential gradient was 329 V cm^{-1}. The space step was 0.0002 cm for the solid line and 0.05 cm for the broken line. For other simulation conditions, see text.

zones existed before and behind the sample peaks, and the peak profile itself was distorted by a non-physical shoulder peak. On the other hand, in the present simulation, no negative concentration zones were generated and the peak profile of each sample retained correct shape with no distortion, as is obvious from Fig. 2. Half widths of pyridine and aniline were 0.12 and 0.24 min, respectively, and the values agreed well with those of the previous method [7]. However, the base of each peak was slightly broadened instead of forming a negative zone. Thus, it was concluded that high numerical stability was achieved in our simulation using 'shifted upwinding' approximation. The most characteristic point of the present simulation is that non-physical peaks are hardly generated. In fact, even when a 6-fold larger current was applied in the above calculation, non-physical peaks did not appear.

The dashed line in Fig. 2 shows the electropherogram simulated for the same samples under the same conditions except for a space step of 0.01 cm being used instead of 0.002 cm. The time necessary for the calculation was 25 h, which was one-fifth the time of previous calculations (135 h). Although non-physical peaks were not generated, such rapid calculation overestimates the ionic diffusion: in this case the half-width of the peak increased as 0.22 min for pyridine and 0.33 min for aniline.

Table 2 shows comparison of the simulation performance between previously reported programs [7] and ours. Although non-physical peaks hardly appeared in our simulation, they were more or less generated in the previous simulations. Half widths of sample peaks were the same as obtained by the simulation of Ermakov et al. [7], but numerical dispersion seemed to be slightly larger than theirs. Calculation oscillated easily in the simulations of Dose and Guichon [5] and Mosher et al. [2], while

Table 2
Comparison of simulation behavior among various simulation programs

Methods	Non-physical peak	Numerical dispersion	Oscillation	Divergence	Current density
Dose and Guichon [5]	Poor	Poor	Poor	Poor	Low
Mosher et al. [2]	Poor	Poor	Poor	Fair	Medium
Ermakov et al. [7]	Good	Good	Good	Good	High
This work	Excellent	Fair	Good	Good	High

no obvious oscillation appeared in our simulation or that of Ermakov et al [7]. No divergence appeared in our method, even in the case of high current density. Obviously, the simulation performance of our program is the most sophisticated at present.

5.2. Rapid simulation by applying high potential gradient

Since numerical stability is high in our simulation program, the migration process of CZE can be analyzed rapidly under the calculation conditions of high potential gradient, large space step and time step. As an example of a rapid simulation by applying high potential gradient, a simulation was carried out assuming a potential gradient of 750 V cm^{-1}. The sample was an equimolar mixture of ϵ-aminocaproic acid, LiCl and KCl as described in Section 2. The space step of 0.05 cm was used for the rapid calculation, which was much greater than the value of 0.002 cm for Fig. 2.

When the Dose and Guichon [5] upwinding approximation was used, the calculation diverged. Obviously from the total sample amount shown in Table 3, the concentration of all sample ions increased with time, and consequently this simulation stopped at $t=0.690$ s. Even under a mild calculation condition, simulation erroneously terminated. For example, when the potential gradient was decreased to 250 V cm^{-1}, the space step was 0.0001 cm, and the time step was 0.001 s, the simulation program stopped at $t=1.90$ s.

On the other hand, no divergence was observed in our simulation, as is obvious from Table 3. As a result of the large space step (0.05 cm), it took rather a short time (ca. 24 h) to simulate the migration process for 100 s. Fig. 3 shows the peak profiles of ϵ-aminocaproic acid and chloride ion in the initial stage of migration process. Non-physical peaks were not generated and it was suggested that the chloride ion played an important roll in determining the initial concentration of the sample ion.

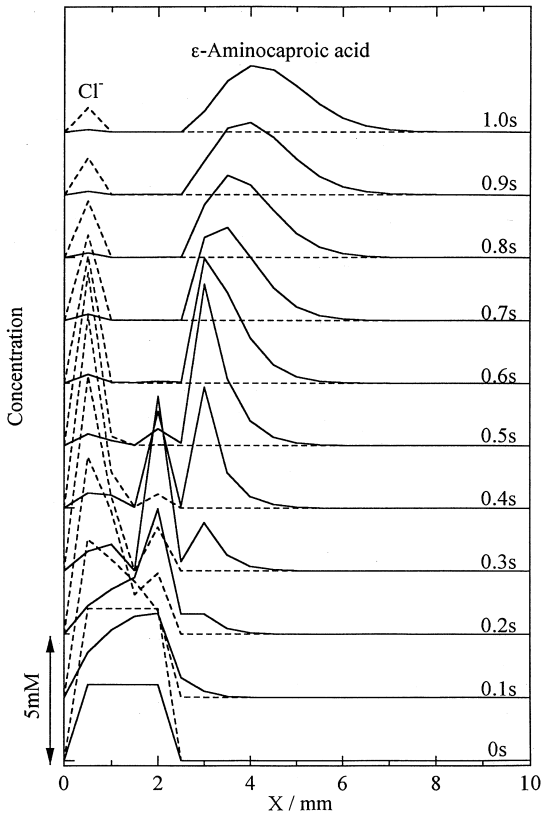

Fig. 3. Simulated concentration profiles of aminocaproic acid (solid line) and chloride ion (broken line) in the initial stage of the CZE process. The potential gradient was 750 V cm^{-1}. The space step was 0.05 cm. For other simulation conditions, see text.

Fig. 4 shows concentration profiles of three sample ions at 1 and 10 s after starting migration. Since the numerical dispersion was large in such a

Table 3
The total amounts of samples in simulations (m*M* cm)

Algorithm	Sample	0 s	0.1 s	0.2 s	0.3 s	0.4 s	0.5 s	0.6 s	50 s
Dose's winding	K	0.60000	0.55545	11.148	147.67	680.24	1447.33	1535.5	—
	Li	0.60000	0.52243	3.3141	61.822	396.47	944.385	1005.1	—
	ϵ-Aminocaproic acid	0.60000	0.55720	0.72590	2.2338	7.3331	14.3939	15.393	—
Shifted upwinding	K	0.60000	0.60000	0.60000	0.60000	0.60000	0.60000	0.60000	0.60000
	Li	0.60000	0.60000	0.60000	0.60000	0.60000	0.60000	0.60000	0.60000
	ϵ-Aminocaproic acid	0.60000	0.60000	0.60000	0.60000	0.60000	0.60000	0.60000	0.60000

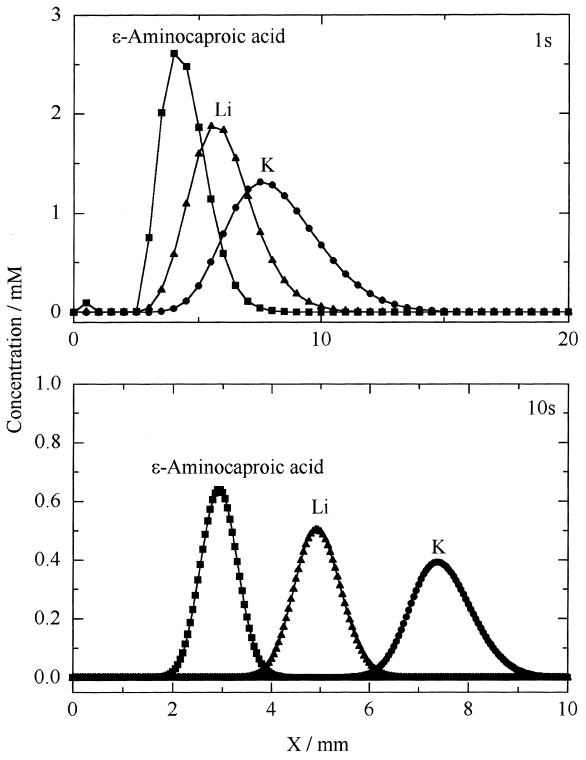

Fig. 4. Simulated concentration profiles of ϵ-aminocaproic acid, LiCl and KCl in the CZE process at 1 and 10 s after starting migration. The space step was 0.05 cm.

rapid calculation, the peak profiles were symmetric already at 10 s after starting migration. When accurate peak profiles are necessary at the cost of calculation speed, a small space step should be selected as $\Delta x \approx D$.

5.3. System peak in indirect UV detection

Fig. 5 shows the simulated concentration profile of creatinine at 100 s after starting migration. In this case creatinine is a visualizing agent for indirect UV detection. The mobility of the system peak was evaluated at 30.0×10^{-5} cm^2 V^{-1} s^{-1} from the simulation. That is, it is just equal to the mobility of EOF used in the simulation. Since the stationary concentration boundary at a sample plug remained at the initial position, the system peak is not the concentration boundary which migrated with EOF, but it is a concentrated or diluted zone of creatinine generated at the boundary. That is, the system peak is not the sample plug evacuated by the samples. Furthermore, the concentration of creatinine fluctuated before and after the system peak confirming the above conclusion.

Fig. 6 shows the concentration profile of creatinine in the initial stage of the migration process. It is clear that the concentrated zone was first

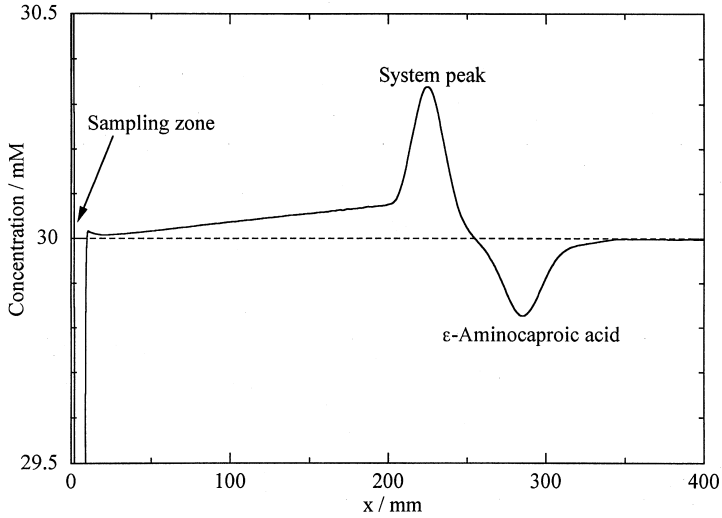

Fig. 5. Simulated concentration profile of creatinine (the visualizing agent) in the CZE process of ϵ-aminocaproic acid, LiCl and KCl (100 s after starting migration). Simulation conditions as in Fig. 4.

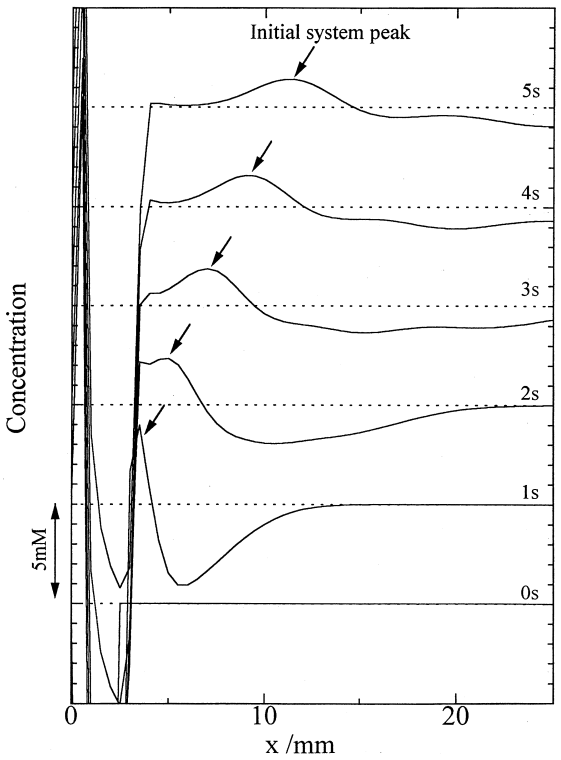

Fig. 6. Concentration profile of creatinine in the initial stage of the CZE process. A pointed peak is the initial system peak. Dotted lines shows 30 m*M* (original concentration of creatinine).

formed near the front end of the sample plug at 1 s after starting migration, and it migrated as diffused with the velocity of EOF. Beckers extensively studied the system peaks in CZE from both a theoretical and an experimental viewpoint [10]. His conclusion was that a system peak was a change in the concentration generated at the stationary concentration boundary, which was in good agreement with our simulation.

The above conclusion can be derived because our simulation hardly generates any non-physical peaks during the migration process, even under high potential gradient. Thus, our simulation program with a 'shifted upwinding' approximation will be useful for the prediction of the initial stage of the migration process in CE. We will report how the migration time is affected by the nature of the sample solution in the following paper.

References

[1] R.A. Mosher, D.A. Saville, W. Thormann, The Dynamics of Electrophoresis, VCH, Weinheim, 1992.
[2] R.A. Mosher, D. Dewey, W. Thormann, D.A. Saville, M. Bier, Anal. Chem. 61 (1989) 362.
[3] B. Gas, J. Vacik, I. Zelensky, J. Chromatogr. 545 (1991) 225.
[4] E. Durovcakovam, B. Gas, J. Vacik, E. Smolkova Keulemansova, J. Chromatogr. 623 (1992) 337.
[5] E.V. Dose, G.A. Guichon, Anal. Chem. 63 (1991) 1063.
[6] S.V. Ermakov, O.S. Mazhorova, M.Yu. Zhukov, Electrophoresis 13 (1992) 838.
[7] S.V. Ermakov, M.S. Bellp, P.G. Righetti, J. Chromatogr. A 661 (1994) 265.
[8] F. Kohlrausch, Ann. Phys. Chem. 62 (1897) 209.
[9] F.E.P. Mikkers, F.M. Evaraerts, Th.P.E.M. Verheggen, J. Chromatgr. 169 (1979) 1.
[10] J.L. Beckers, J. Chromatogr. A 662 (1994) 153.